Epileptic brain fluorescent imaging reveals apigenin can relieve the myeloperoxidase-mediated oxidative stress and inhibit ferroptosis

Chenwen Shao[a,b,1], Jiwen Yuan[b,1], Yani Liu[b], Yajuan Qin[c], Xueao Wang[b], Jin Gu[b], Guiquan Chen[d], Bing Zhang[e], Hong-Ke Liu[a], Jing Zhao[b,2], Hai-Liang Zhu[b,2], and Yong Qian[a,b,2]

[a]School of Chemistry and Materials Science, Nanjing Normal University, 210046 Nanjing, China; [b]State Key Laboratory of Pharmaceutical Biotechnology, School of Life Sciences, Nanjing University, 210023 Nanjing, China; [c]School of Pharmacy, Nanjing Medical University, 211166 Nanjing, China; [d]State Key Laboratory of Pharmaceutical Biotechnology, Model Animal Research Center, Nanjing University, 210061 Nanjing, China; and [e]Department of Radiology, The Affiliated Drum Tower Hospital of Nanjing University Medical School, 210008 Nanjing, China

Edited by Gregory A. Petsko, Brigham and Women's Hospital, Boston, MA, and approved March 18, 2020 (received for review October 16, 2019)

Myeloperoxidase (MPO)-mediated oxidative stress has been suggested to play an important role in the pathological dysfunction of epileptic brains. However, there is currently no robust brain-imaging tool to detect real-time endogenous hypochlorite (HClO) generation by MPO or a fluorescent probe for rapid high-throughput screening of antiepileptic agents that control the MPO-mediated chlorination stress. Herein, we report an efficient two-photon fluorescence probe (named HCP) for the real-time detection of endogenous HClO signals generated by MPO in the brain of kainic acid (KA)-induced epileptic mice, where HClO-dependent chlorination of quinolone fluorophore gives the enhanced fluorescence response. With this probe, we visualized directly the endogenous HClO fluxes generated by the overexpression of MPO activity in vivo and ex vivo in mouse brains with epileptic behaviors. Notably, by using HCP, we have also constructed a high-throughput screening approach to rapidly screen the potential antiepileptic agents to control MPO-mediated oxidative stress. Moreover, from this screen, we identified that the flavonoid compound apigenin can relieve the MPO-mediated oxidative stress and inhibit the ferroptosis of neuronal cells. Overall, this work provides a versatile fluorescence tool for elucidating the role of HClO generation by MPO in the pathology of epileptic seizures and for rapidly discovering additional antiepileptic agents to prevent and treat epilepsy.

brain imaging | fluorescent probe | myeloperoxidase | epilepsy

Myeloperoxidase (MPO) is a peroxidase enzyme containing two molecules of iron that catalyzes the conversion of hydrogen peroxide and chloride ions to release more cytotoxic hypochlorite (HClO) (pK_a 7.6) and other chlorinated species, leading to potential oxidative stress (1). The strong oxidizing and chlorinating ability of HClO plays an important role in the immunity against pathogens (2, 3). However, overexpressing of MPO and its mediated oxidative stress could contribute to inflammation, severe tissue damage, and neurological disorders (4). Mounting evidence suggests that there is close crosstalk between the abnormally elevated MPO and neurodegenerative diseases, such as Alzheimer's disease (AD), Parkinson's disease (PD), Huntington's disease (HD), stroke, depression, and epilepsy (5–9). Moreover, some current studies have shown that an increase in the levels of MPO is associated with epileptogenesis (10), suggesting that MPO might be a promising biomarker for the early diagnosis of epilepsy and could also serve as a potential therapeutic target for epilepsy (11). Therefore, defining dynamic changes of MPO activity and its mediated chlorinated stress will help to better understand the potential molecular mechanism underlying epileptic seizures. However, the detailed changes and regulation of MPO dynamical activity during epileptogenesis have not been fully elucidated. Thus, the direct visualization of MPO-mediated oxidative stress in vivo and rapid screening of efficient lead compounds for epilepsy treatment remain highly desirable but challenging.

Because of the unique advantages of fluorescent imaging, including high sensitivity and selectivity, simplicity, excellent spatiotemporal resolution, and noninvasive visualization, activity-based sensing probes have been considered as desirable and indispensable tools for mapping reactive oxygen species in living biosystems (12–20). Until now, some fluorescent probes have been reported that can be successfully used for the determination of HClO in vitro and imaging HClO in living cells (21–24). However, most of these one-photon fluorescent probes are limited by their short excitation wavelengths, poor tissue permeability, and photobleaching. To address these limitations, a potential approach is to develop two-photon fluorescent probes for two-photon fluorescence microscopy (TPM). By using two-photon excitation with near-infrared (NIR) light, it is possible to perform three-dimensional (3D) visualization of biological samples with deeper tissue imaging, less photobleaching, less background fluorescence, and higher temporal–spatial resolution (25–29). To date, few two-photon fluorescent probes

Significance

Endogenous hypochlorite (HClO), the strong oxidizing and chlorinating species generated by myeloperoxidase, has been speculated to be closely associated with the development of epilepsy. However, direct imaging evidence from live brains with epileptic behaviors is rare. Herein, we have developed a two-photon fluorescence probe for the real-time tracking of endogenous HClO fluxes in vivo and ex vivo in epileptic brains. The application of this probe to construct a high-throughput screening platform would rapidly screen the potential antiepileptic agents to control overexpressing HClO. This work provides a versatile chemical tool for investigating HClO under pathological conditions of epilepsy and could be used to rapidly discover additional antiepileptic agents.

Author contributions: Y. Qian designed research; C.S., J.Y., Y.L., and Y. Qin performed research; J.Y., X.W., J.G., G.C., B.Z., H.-K.L., J.Z., and H.-L.Z. contributed new reagents/analytic tools; C.S., Y.L., Y. Qin, X.W., J.G., and Y. Qian analyzed data; J.Z., H.-L.Z., and Y. Qian supervised the study; and C.S. and Y. Qian wrote the paper.

Competing interest statement: Nanjing Normal University has filed a patent on the technique described herein that lists Y. Qian and C.S. as inventors.

This article is a PNAS Direct Submission.

[1]C.S. and J.Y. contributed equally to this work.

[2]To whom correspondence may be addressed. Email: yongqian@njnu.edu.cn, jingzhao@nju.edu.cn, or zhuhl@nju.edu.cn.

This article contains supporting information online at https://www.pnas.org/lookup/suppl/doi:10.1073/pnas.1917946117/-/DCSupplemental.

First published April 23, 2020.

have been developed for imaging HClO in live cells (30–36). With these probes, visualization of HClO in wounded tissues or an inflammatory mouse model has been achieved (35, 37). However, there has been no report on direct real-time visualization of HClO fluxes in the brain of live animals, especially during epileptic seizures. Moreover, no fluorescent probe is currently available for high-throughput screening of antiepileptic agents to control MPO-mediated oxidative stress. To meet these demands, there are great challenges for the development of brain-imaging agents, including effective blood–brain barrier (BBB) penetrability, high specificity, good sensitivity, and desired photophysical properties (38–40). Thus, development of a two-photon fluorescent probe for imaging MPO-mediated oxidative stress in the brain with epilepsy-like behaviors and for high-throughput screening of antiepileptic agents is urgently needed.

Herein, we report an efficient two-photon fluorescent probe, named HCP, for the real-time detection of endogenous HClO signals generated by MPO in vivo in mouse brains of kainic acid (KA)-induced epileptic seizure and for constructing a high-throughput screening approach to screen antiepileptic agents to control MPO-mediated oxidative stress. This probe was rationally designed using a simple condensation between 6-(dimethylamino)quinoline-2-carbaldehyde and diaminomaleonitrile, exhibiting two-photon excitability, BBB penetrability, and high sensitivity and selectivity toward MPO-generated HClO in live cells and in vivo. The HCP itself displays only a weak yellow fluorescence, while the chlorinated derivative (HCP-Cl), which can be rapidly formed after reaction with HClO (Scheme 1), gives a bright green fluorescence enhancement (almost 138-fold). Using this probe, the detection and imaging of HClO generation by MPO in epileptic brains are demonstrated in vivo and ex vivo (*SI Appendix*, Table S1). Importantly, in combination with high-content analysis (HCA) and HCP, a simple and efficient high-throughput screening (HTS) platform was first developed for screening antiepileptic agents to efficiently control the release of MPO-generated HClO and chlorinated stress in live cells. In particular, by two-photon fluorescence imaging with HCP, it was directly observed that the screened lead compound apigenin effectively controlled the MPO-generated HClO levels under KA-induced stress in live brains, which subsequently led to the direct observation of enhanced antioxidant capability in apigenin-activated neural cells. Furthermore, detailed mechanism studies have further confirmed that apigenin can efficiently reduce the expression of intracellular MPO and increase the levels of GPX4 and SIRT1, thereby conferring neuroprotection through regulation of KA-induced ferroptosis. This strategy will allow real-time tracking HClO generation by MPO in epileptic brains in vivo and rapid discovery of additional antiepileptic agents by the HTS strategy, which could uncover additional mechanisms in the chemical regulation of epileptic seizures.

Results and Discussion

Probe Design and Synthesis. To achieve the real-time detection of HClO generation by MPO in live brains in animal models, the designed activity-based sensing probe should be noncytotoxic, have BBB penetrability, and have bright fluorescence. Taking into account the properties of the various fluorophores, the quinoline skeleton has attracted our great interest because of its drug-like physicochemical and photophysical properties. Previously, the quinoline derivatives have shown that the desired BBB penetrability can be applied for the development of brain imaging or neuroprotective agents (41–45). For example, a quinolone-based Schiff base can serve as a staining reagent for imaging metal ions (Cu^{2+} and Zn^{2+}) in Aβ plaques; quinolylnitrones can be used as the potential neuroprotective agents (*SI Appendix*, Scheme S1). Moreover, the quinoline skeleton has excellent two-photon excitation properties that enable the design of two-photon fluorescent probes for deep tissue imaging in living organisms (20, 30, 46). Inspired by these quinolone-based neuroprotective drugs and imaging agents, we sought a simple condensation reaction to construct a two-photon fluorescent probe based on the principle of intermolecular charge transfer (ICT) (47). Thus, probe HCP was designed and synthesized by a Schiff base functionalized 6-(dimethylamino)quinolone-2-carbaldehyde with a diaminomaleonitrile (*SI Appendix*, Scheme S2). In HCP, the conjugated electron-acceptor diaminomaleonitrile group weakens the push–pull electron effect of quinolone fluorophore, thereby resulting in a weak yellow fluorescence. In the presence of HClO, the structural modification of HCP to form HCP-Cl will be expected by a chlorination reaction, thus altering the intermolecular electronic effect to achieve the blue-shifted emission enhancement (Scheme 1 and *SI Appendix*, Fig. S1). We envision that this probe should give an obvious fluorescence response to MPO-generated HClO under two-photon excitation. Based on this idea, the probe HCP was prepared straightforward from commercially available starting materials according to *SI Appendix*, and its structure was fully characterized by ^{1}H and ^{13}C NMR spectroscopy and high-resolution mass spectrometry (HR-MS). The two-photon properties of HCP in the absence

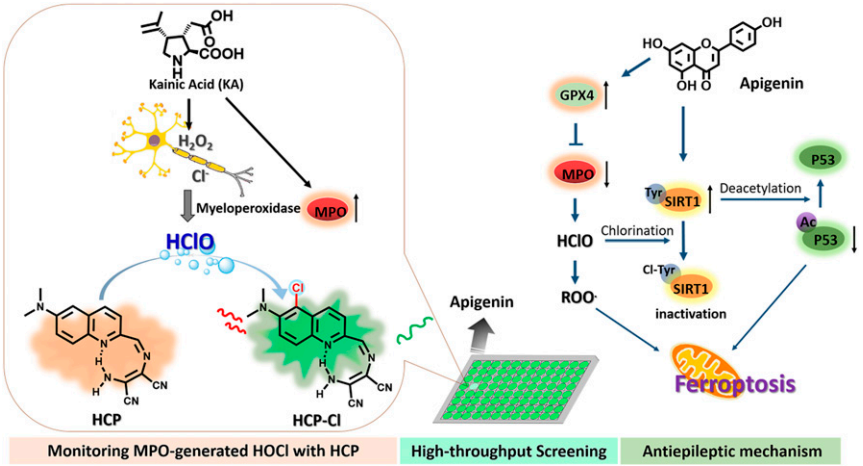

Scheme 1. Design of a two-photon fluorescent probe, HCP, for monitoring of MPO-generated HClO in KA-induced epilepsy and demonstration of the strategy for high-throughput screening of antiepileptic agents.

and presence of HClO were investigated by detecting its two-photon absorption cross-section (δ_2). We observed an apparent increase in δ_2 values after incubation with HClO upon excitation from 730 to 830 nm. We also observed the maximum δ_2 values of about 13.4 GM at 800 nm (~8.2-fold enhancement) (Fig. 1*A* and *SI Appendix*, Fig. S2). These findings confirmed the suitability of HCP for two-photon imaging.

Spectral Response of HCP to HClO In Vitro. The spectroscopic properties of HCP were first examined in PBS (10 mM, pH 7.4, 5% dimethyl sulfoxide [DMSO]); the HCP (Φ, 0.025) itself displays a maximal absorption peak at 451 nm and fluorescence peak at 581 nm upon excitation at 390 nm (Fig. 1 *B* and *C*). To test the responses of HCP toward HClO, the absorption and fluorescence spectral analyses were performed under physiological conditions. After the addition of HClO, the absorption and fluorescence peaks of HCP decreased markedly, while the characteristic blue-shifted absorption and fluorescence emission peaks emerged at 396 and 495 nm, respectively. Time-dependent fluorescence studies revealed that the enhancement of fluorescence intensity was extremely fast within 5 s (Fig. 1*D*), exhibiting ca. 138-fold enhancement in the fluorescence intensity after reaction with HClO. High-performance liquid chromatography–mass spectrometry (HPLC-MS) analysis of the reaction mixture further confirmed the formation of a chlorinated product (HCP-Cl) as the major product, which is consistent with the probe design and ^{1}H-NMR analytic results (*SI Appendix*, Fig. S1).

The specificity of HCP was studied by investigating the fluorescent response upon the addition of various analytes. As shown in Fig. 1*E*, HCP exhibited excellent selectivity toward HClO over other biologically relevant molecules, such as other competitive reactive oxygen or nitrogen species (ROS/RNS) ($^{\bullet}OH$, $^{\bullet}O_2^-$, $^1O_2$, H_2O_2, OBr^-, TBHP, $ONOO^-$, NO, NO_2^-, and NO_3^-), biothiols (H_2S, GSH, and Cys), and metal ions (Cu^{2+}, Fe^{3+}, and Zn^{2+}). Only HClO promoted a remarkable enhancement in emission at 495 nm, whereas no significant change of fluorescence spectra of HCP was observed in the presence of other interfering species, even at higher concentration (10 equivalent). HCP exhibited >40-fold and >80-fold selectivity for HClO over other species in the enhancement of fluorescence intensity at 495 nm. It should be noted that hypobromous acid (HBrO) (pK_a 8.8) can also be generated by eosinophil peroxidase (EPO) even at physiological conditions, where a 1,000-fold excess of chloride over bromide ([Cl^-] 140 mM, [Br^-] 20 to 100 μM) (48). Thus, the anti-interference of HCP toward HBrO was further investigated in the presence of both HClO (100 μM) and HBrO (100 μM) by fluorescence analysis, demonstrating that the significant fluorescence enhancement can only be promoted by HClO (*SI Appendix*, Fig. S3). Although a large excess of HBrO (>200 μM) can result in a weak fluorescence enhancement of HCP, positive response elicited by HBrO would not take place within the physiologically relevant concentrations ([HBrO] <<100 μM), even with much longer incubation time (60 min), suggesting that the interference from HBrO is negligible.

To identify the sensitivity of HCP toward HClO, the enhancement of fluorescence intensity at 495 nm was investigated with increasing HClO concentration within the measured range (0 to 50 μM) (Fig. 1*F*). As expected, the fluorescence intensity was found to increase gradually, leveling off after treatment with 3 equivalent of HClO with a ca. 122-fold enhancement of fluorescence intensity at 495 nm. An excellent linear relationship was observed between the fluorescence intensity at 495 nm and the low concentration of HClO in the range of 0 to 15 μM (R^2 = 0.9814) (*SI Appendix*, Fig. S4); the limit of detection (LOD) for HClO using HCP was determined to be 104 nM. To the naked eye, these corresponded to a remarkable color change from brown to gray-blue under hand-held UV lamp irradiation (365 nm) and pale yellow to colorless under visible light (Fig. 1 *G*, *Inset* and *SI Appendix*, Fig. S5).

In addition, to further determine the stability of HCP toward variations of pH microenvironments, we performed reactions at different pH conditions from 3 to 12. As displayed in *SI Appendix*, Fig. S6, HCP remained stable and detectable over a wide pH range, even under acidic or alkaline conditions. Importantly, HCP exhibited significant fluorescence response toward HClO in

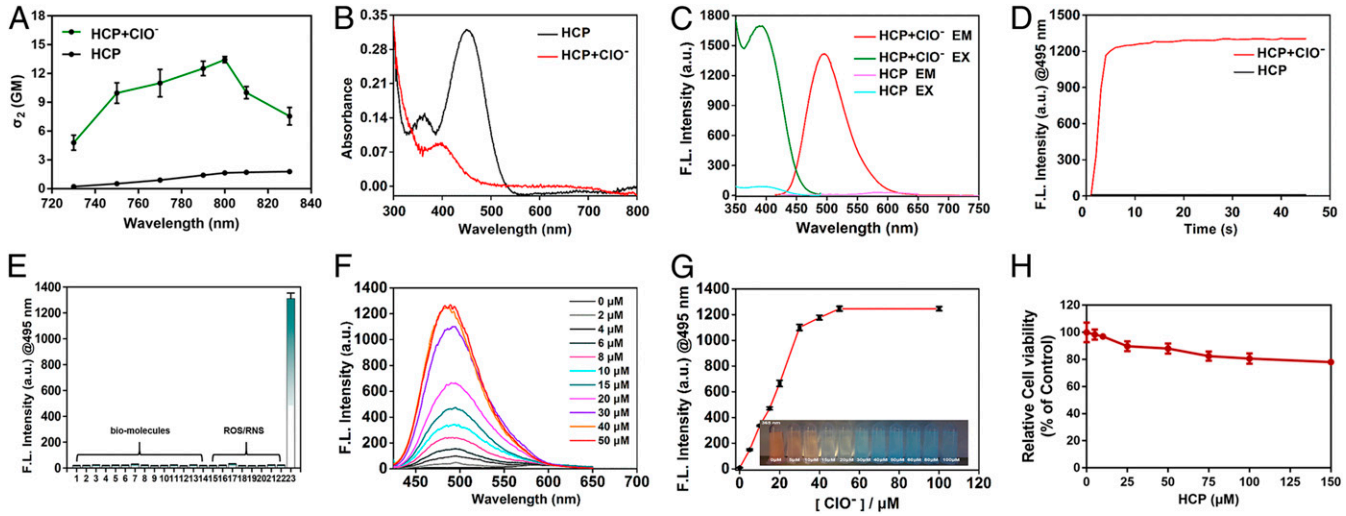

Fig. 1. Evaluation of HCP for the detection of HClO in vitro. (*A*) Two-photon action spectra of HCP (10 μM) in the absence (black) and presence (green) of ClO^- (100 μM) upon excitation from 730 to 830 nm. (*B*) The absorption spectra of HCP (10 μM) in the absence or presence of ClO^- (50 μM) in PBS buffer (10 mM, pH 7.4, 5% DMSO). (*C*) The excitation spectra (EX) and emission spectra (EM) of HCP (10 μM) before and after adding ClO^- (50 μM). (*D*) Time course of fluorescence intensity of HCP (10 μM) at 495 nm before and after adding ClO^- (50 μM). (*E*) Fluorescence intensity of HCP (10 μM) at 495 nm in the presence of various analytes (50 μM for biomolecules [2 to 14] and 100 μM for other ROS/RNS [15 to 22]: 1, PBS; 2, Fe^{3+}; 3, Zn^{2+}; 4, Cu^{2+}; 5, SO_3^{2-}; 6, PO_4^{3-}; 7, NO_3^-; 8, Cl^-; 9, Br^-; 10, H_2S; 11, GSH; 12, Cys; 13, V_C; 14, NO_2^-; 15, NO; 16, $^{\bullet}OH$; 17, H_2O_2; 18, TBHP; 19, $O_2^{\bullet-}$; 20, $ONOO^-$; 21, $^1O_2$; 22, BrO^-; 23, ClO^-). (*F*) Fluorescence enhancement of HCP (10 μM) as a function of ClO^- (0 to 50 μM) in PBS buffer at 37 °C. (*G*) Concentration-dependent changes in the fluorescence intensity of HCP (10 μM) at 495 nm in PBS buffer at 37 °C. HCP (10 μM) was incubated with different concentrations of ClO^- (0, 5, 10, 15, 20, 30, 40, 50, 60, 80, and 100 μM) at room temperature, and the photographs were taken under 365 nm UV. (*H*) The cell viability of SH-SY5Y cells treated with different concentrations of HCP (0 to 150 μM) for 48 h. All data are presented as the mean ± SD (n = 3 to 5).

the physiological pH range (6.0 to 8.5), strongly suggesting that HCP can work in physiological contexts. To evaluate the cytotoxicity of HCP toward human neuroblastoma SH-SY5Y cells, we performed Cell Counting Kit-8 (CCK-8) assays after treatment with increasing concentrations of HCP for 48 h, suggesting HCP had nearly no cytotoxicity even at 150 μM (Fig. 1*H*). Moreover, the photostability of HCP was also examined in live cells, suggesting excellent photostability and good performance for long-term traceability in live cells (*SI Appendix*, Fig. S7). Taken together, these observations confirmed the excellent selectivity and sensitivity and rapid response of HCP toward HClO, thereby suggesting the potential of HCP as an efficient tool for real-time tracking of HClO in complex biological contexts.

Fluorescent Response of HCP to Dynamic Changes of HClO in Living Cells. To explore the capability of HCP for HClO detection in live cells, living SH-SY5Y cells were pretreated with different concentrations of exogenous HClO (0 to 50 μM), and images were taken to observe the HCP fluorescence response toward HClO by high-content analysis after incubation with 10 μM HCP. As presented in Fig. 2, the HCP-loaded cells showed weak green fluorescence signals in the absence of the exogenous HClO; upon exposure to increasing concentrations of exogenous HClO, intracellular fluorescence gradually increased in a concentration-dependent manner. Compared to the control group, the addition of 50 μM HClO resulted in at least two-fold enhancement of fluorescence intensity, suggesting that HCP can effectively penetrate the cell membrane and detect the exogenous change of HClO levels (Fig. 2 *A* and *B*).

To ask whether HCP had the potential capability for imaging endogenous HClO in living cells, lipopolysaccharide (LPS), an inflammation activator, was applied to stimulate cells to generate endogenous HClO. Cells were pretreated with LPS (1 μg/mL) for 12 h and then incubated with HCP (10 μM) for another 30 min. A robust fluorescence enhancement was more clearly observed in the LPS-treated group than in the control. To ensure the fluorescence enhancement as a result of endogenous HClO generation by MPO, cells were preincubated with MPO\-H_2O_2\$Cl^-$ and then incubated with HCP. A remarkable increase in fluorescence intensity was observed in the MPO-treated group, while H_2O_2\$Cl^-$ alone did not promote an obvious change of fluorescence intensity. In contrast, drug-treated cells with 4-aminobenzoic acid hydrazide (4-ABAH) or salicylhydroxamic acid (SHA) (well-known inhibitors of MPO) exhibited much weaker fluorescence in the green channel compared to the untreated group, clearly suggesting the inhibition of MPO activity induced decrease of intracellular HClO generation (Fig. 2 *C* and *D*). Collectively, these data indicate that HCP is applicable for real-time detecting and imaging of HClO generation by MPO in live cells and suggest its promise for serving as a simple tool to explore dynamic changes of endogenous HClO levels at the different states of cellular microenvironments under high-content analysis.

High-Throughput Screening of Natural Products with HCP. Motivated by the excellent performance of HCP for live-cell imaging, we next moved on to evaluate whether HCP can serve as an effective identification tool for screening the potential antioxidant against HClO formation (Fig. 3). We first explored a simple and effective fluorescence-based high-throughput screening platform by using HCP in combination with HCA. Next, live SH-SY5Y cells were pretreated with 20 μM different natural products that exhibited potential antioxidative activities for 12 h, and images and quantitative analysis of endogenous HClO were followed by HCA after incubation of 10 μM HCP. This approach ensured that the endogenous HClO generation could be detected rapidly and quantitatively. We found that most of these selected natural products could induce the important decrease of fluorescence signals, thus suggesting the down-regulation of HClO generation. Importantly, apigenin, a classic flavonoid (49), was observed that can efficiently blunt the fluorescence signals when compared with the untreated control, suggesting that this flavonoid compound could be a potential agent for controlling the accumulation of MPO-generated HClO in live cells (*SI Appendix*, Figs. S8 and S9). Overall, the HCA screening result first revealed that HCP could be employed as a simple tool to screen lead compounds for regulating endogenous HClO variations in the HCA platform.

Imaging in Live Cells with HCP under Glutamate\Kainic Acid-Induced Oxidative Stress. Oxidative stress, especially HClO produced by MPO, is considered to be highly correlated with neurological disorders (1). To confirm whether HCP could visualize dynamic changes of endogenous HClO under stimulated oxidative stress, we subsequently used HCP to profile simultaneous HClO generation in live neural cells. Previous reports have shown that high concentrations of glutamate supply can induce oxidative stress (50). SH-SY5Y cells were preloaded with glutamate for 12 h and

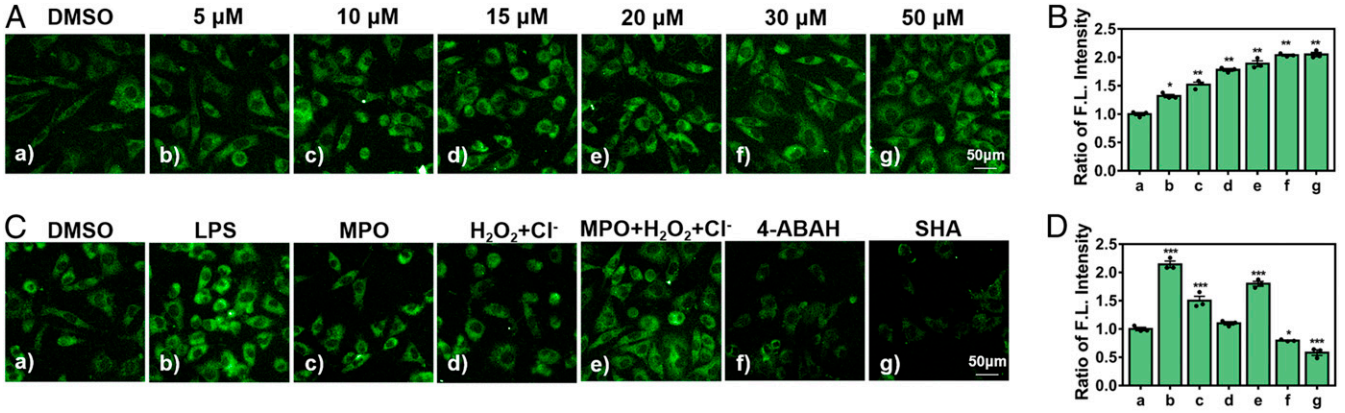

Fig. 2. Imaging HClO fluxes in living SH-SY5Y human neuroblastoma cells with HCP by HCA. (*A*) Cells were pretreated with different concentrations of ClO^- (0, 5, 10, 15, 20, 30, and 50 μM) for 30 min, followed by fluorescence imaging after incubation with HCP (10 μM) in the fresh medium for another 30 min, respectively. (*B*) The relative ratio of fluorescence intensity of the cells shown in *A* was quantified. (*C*) Cells were preincubated with or without LPS (1 μg/mL, 12 h), MPO (100 ng/mL, 1 h), H_2O_2 (100 μM, 1 h), Cl^- (1 mM, 1 h), 4-ABAH (500 μM, 1 h), and SHA (500 μM, 1 h) and then treated with HCP (10 μM) for another 30 min in the fresh medium. After washing with PBS, cells were imaged. The 4-ABAH and SHA are shown as inhibitors of MPO. (*D*) Effects of different stimuli on changes in HCP fluorescence in *C* that were quantified. Images were obtained using 380 nm for HCP excitation; fluorescence emission, 500 to 550 nm. (Scale bar, 50 μm.) The fluorescence intensity of DMSO-treated SH-SY5Y cells stained with HCP was set as 1. Statistical analyses were performed with one-way ANOVA with multiple comparisons: $*P < 0.05$, $**P < 0.01$, $***P < 0.001$ vs. DMSO-treated cells. Error bars are ± SEM ($n = 3$).

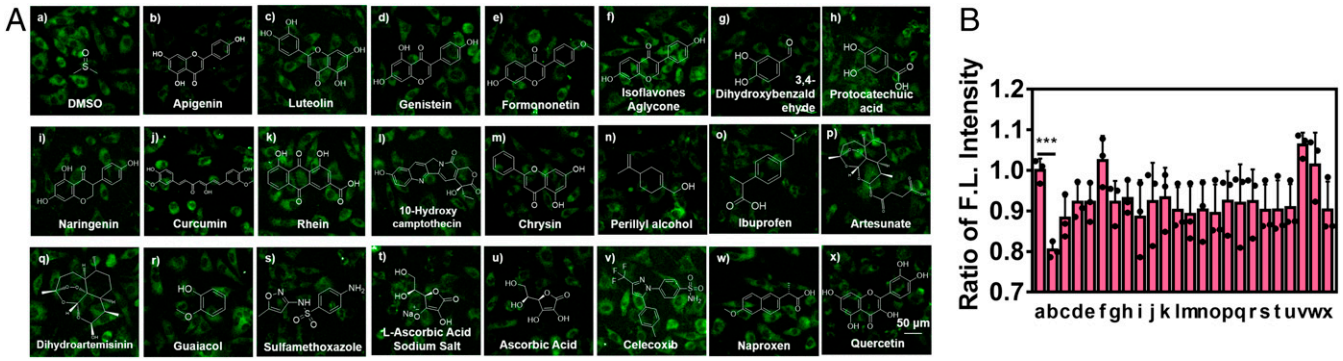

Fig. 3. High-throughput screening of natural products with HCP in living SH-SY5Y human neuroblastoma cells for controlling MPO-mediated oxidative stress. (*A*) Cells were pretreated with various natural antioxidants for 12 h, and then images were acquired by high-content analysis after incubation with HCP (10 μM) for another 30 min. (Scale bar, 50 μm.) (*B*) The relative ratio of fluorescence intensity shown in *A* was quantified. The fluorescence intensity of the DMSO-treated group was set as 1. Images were obtained using 380 nm for HCP excitation; fluorescence emission, 500 to 550 nm. Statistical analyses were performed with one-way ANOVA with multiple comparisons; $*P < 0.05$ vs. DMSO-treated group. Error bars are ± SEM ($n = 3$).

then incubated with HCP for another 30 min. Compared to the control, glutamate-treated cells showed much brighter fluorescence than that of the negative control (Fig. 4 *A* and *B*), suggesting a high sensitivity of HCP to the elevated oxidative stress. To explore whether this enhanced fluorescence of HCP was due to the capture of MPO-generated HClO, we further utilized MPO inhibitors (4-ABAH or SHA) in cells stimulated with glutamate. Compared to the positive glutamate group, weak fluorescence was observed in both MPO inhibitor-treated groups, which was similar to that in the untreated negative control group. Stimulation with KA, a glutamate analog as well as a widely used epilepsy-inducing reagent (51), displayed a concentration-dependent enhancement of fluorescence (Fig. 4*C*). These data first directly showed that the endogenous HClO in human neuronal cells would be generated in excess upon stimulation with glutamate and its analog KA. To determine whether the screened apigenin could effectively control the overexpressing HClO under KA-induced oxidative stress, cells were pre/posttreated with apigenin in KA-stimulated conditions. Surprisingly, the results showed that apigenin obviously inhibited the formation of intracellular HClO during KA-stimulated oxidative stress, which was comparable to that of the positive MPO inhibitors (4-ABAH/SHA) (Fig. 4 *B* and *D* and *SI Appendix*, Fig. S10). Additionally, these findings were further confirmed by flow cytometry analysis and fluorescent imaging using other reported HClO probes (Gal-NAP, C7, R6G), suggesting the change of fluorescence intensity was obviously triggered by endogenous HClO in live SH-SY5Y cells (*SI Appendix*, Fig. S11). Taken together, using visualization by fluorescence imaging with HCP, endogenous HClO generation by MPO responding to external stress can be readily tracked in live cells, and apigenin can be used as a promising agent for controlling MPO-mediated oxidative stress under stimulation.

To further confirm how apigenin relieves KA-induced neuronal stress, we investigated the state of the cell membrane under different stimulation conditions. Fig. 5*A* shows that KA

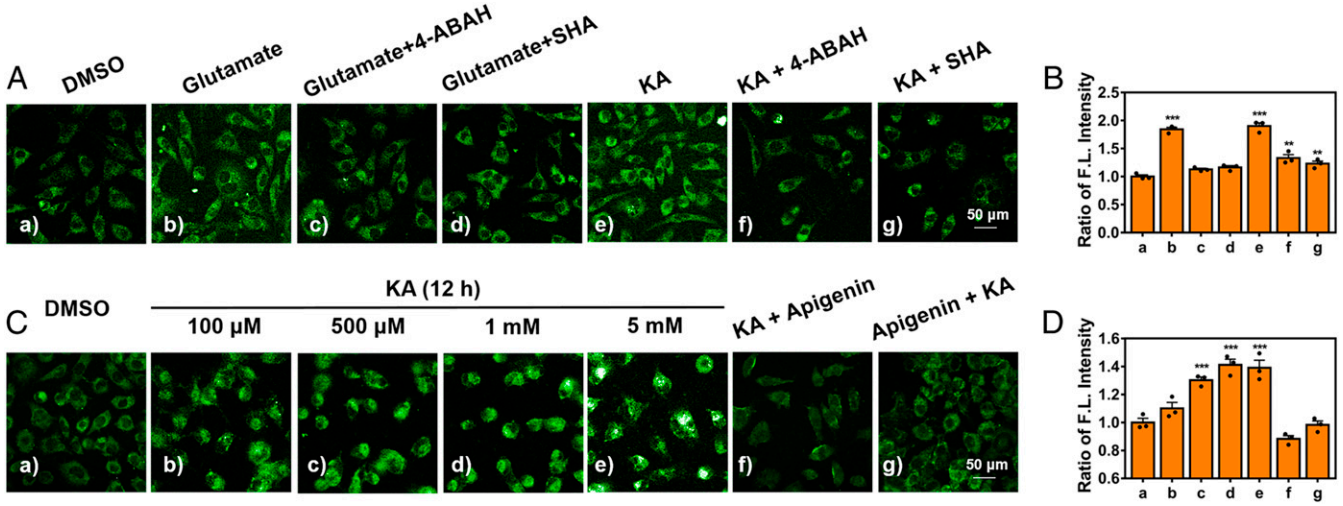

Fig. 4. Fluorescence images of SH-SY5Y human neuroblastoma cells under glutamate/KA-induced oxidative stress. (*A*) Cells were pretreated with or without glutamate (2 mM, 12 h), KA (500 μM, 12 h), 4-ABAH (500 μM, 1 h), and SHA (500 μM, 1 h) and then incubated with HCP (10 μM) for another 30 min in the fresh medium, respectively. (*B*) Relative fluorescence intensities of all SH-SY5Y cells shown in *A* were quantified. (*C*) Cells were preincubated with different concentrations of KA (100 μM, 500 μM, 1 mM, and 5 mM) for 12 h, KA (500 μM,12 h) followed by apigenin (20 μM, 12 h) or apigenin (20 μM, 12 h) followed by KA (500 μM,12 h), and then incubated with HCP (10 μM) for another 30 min in the fresh medium. After cells were washed with PBS, fluorescence images were obtained by high-content analysis. (*D*) The effects of different stimuli on changes in HCP fluorescence in *C* were quantified, and the fluorescence intensity of the DMSO-treated group was set as 1. Images were obtained using 380 nm for HCP excitation; fluorescence emission, 500 to 550 nm. (Scale bar, 50 μm.) Statistical analyses were performed with one-way ANOVA with multiple comparisons. $**P < 0.01$, $***P < 0.001$ vs. DMSO-treated group. Error bars are ± SEM ($n = 3$).

stimulation caused a significant increase in intracellular superoxide, HClO, and lipid peroxidation accumulation compared to the control group. Cotreatment with apigenin can effectively alleviate the overexpressed oxidative stress and show relatively low fluorescence (*SI Appendix*, Fig. S12). Mitochondrial membrane potential imaging by commercial rhodamine 123 dye showed that the KA treatment group effectively reduced the mitochondrial membrane potential, leading to the damage of the mitochondrial membrane; while the membrane potential of the apigenin cotreatment group did not change significantly, compared to the KA-treated alone group (Fig. 5 *B* and *C*). To identify cell populations present in these treated groups, flow cytometric analysis was also performed, and the result was consistent with these fluorescence imaging results, further revealing effective protection of apigenin for the mitochondrial membrane (Fig. 5*D* and *SI Appendix*, Fig. S13). Since the abnormal elevation of lipid peroxidation is one of the important biomarkers of ferroptosis, a nonapoptotic form of cell death involving lipid hydroperoxides (52), we thus envisioned that KA-induced neuronal cell death might be through the ferroptosis pathway. For further validation, Western blotting studies with specific antibodies were performed to observe the expression of GPX4, a key protein regulatory site for ferroptosis (53). The results showed that the expression of GPX4 was significantly decreased under KA stimulation, while the level of GPX4 was importantly increased in the apigenin-treated group (Fig. 5*E* and *SI Appendix*, Fig. S14). Besides, a corresponding change in the MPO expression level was observed. KA treatment promoted the abnormal increase of MPO expression, while cotreatment with apigenin could effectively inhibit the overexpression of MPO. To intuitively observe the structural changes under KA-induced stress, mitochondrial imaging by transmission electron microscopy (TEM) was performed under different treatment conditions (Fig. 5*F*). Compared with the control group, we found that the number of mitochondria in the KA treatment group was significantly reduced, their shape became much smaller, and the internal ridge structure disappeared. Importantly, cotreatment with apigenin could effectively alleviate these phenomena of mitochondrial damage, which is consistent with the corresponding changes in lactic acid production and pyruvate kinase activity (Fig. 5 *G* and *H*).

Moreover, we evaluated the regulatory functions of apigenin in primary neurons, neutrophils, and macrophages, the latter two kinds of cells that might be responsible for the most MPO in the

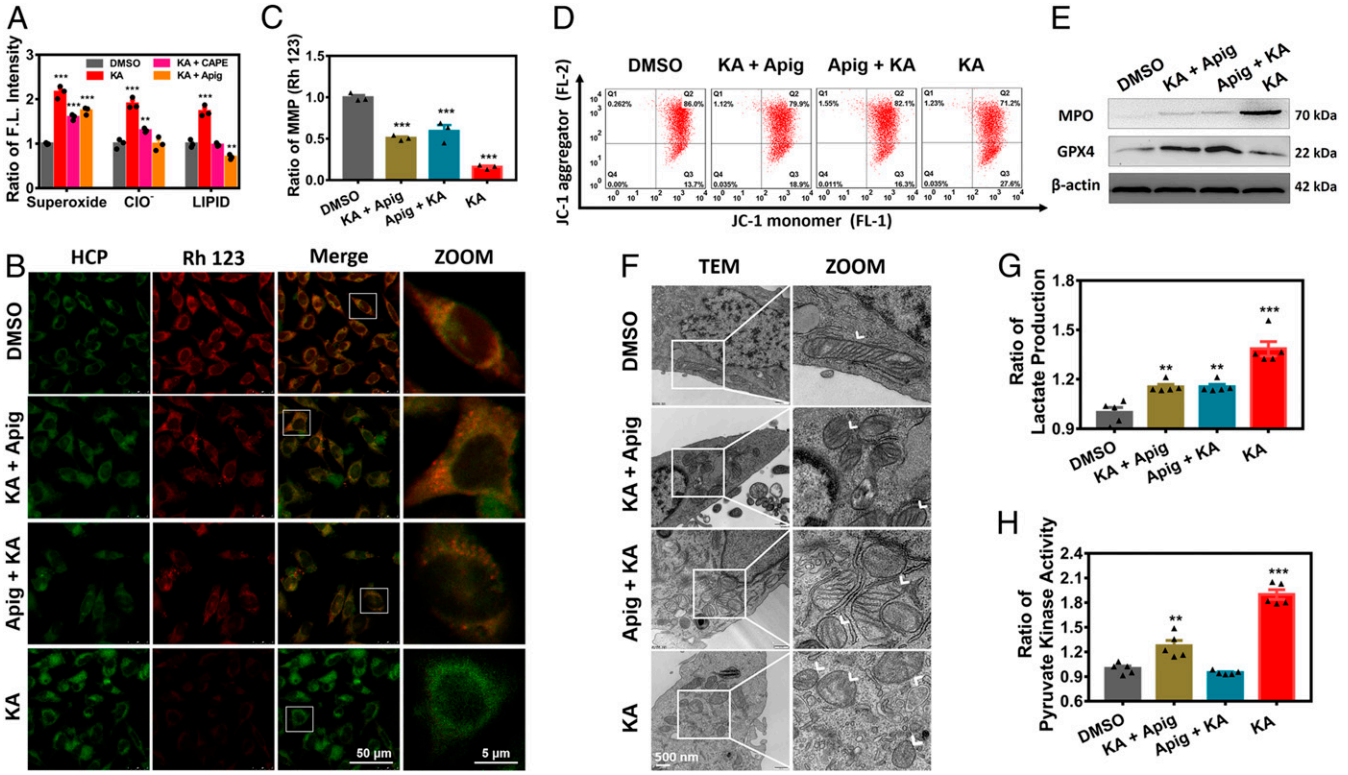

Fig. 5. Investigating the antioxidative ability of apigenin. (*A*) Quantification of the fluorescence signals from dihydroethidium, HCP, and BODIPY 581/591 fluorescence images of SH-SY5Y cells preincubated with or without KA (500 μM, 12 h), CAPE (20 μM, 12 h), and apigenin (20 μM, 12 h). Dihydroethidium channel, excitation = 535 nm, emission = 590 to 640 nm; HCP channel, excitation = 380 nm, emission = 500 to 550 nm; BODIPY 581/591 channel, excitation = 500 nm, emission = 500 to 530 nm. The fluorescence intensity of DMSO-treated cells stained in dihydroethidium, HCP, and BODIPY 581/591 was set as 1, respectively. Error bars are ± SEM (n = 3). (*B*) Fluorescent images of cells stained with rhodamine 123 (10 μM) and HCP (10 μM) that preincubated with or without KA (500 μM, 12 h) and apigenin (20 μM, 12 h). The rhodamine 123 channel, λ_{ex} = 514 nm, λ_{em} = 520 to 570 nm; HCP channel, λ_{ex} = 750 nm, λ_{em} = 450 to 600 nm. (Scale bar, 50 μm; enlarged image scale bar, 5 μm.) (*C*) The fluorescence signals of rhodamine 123 in *B* were quantified. The fluorescence intensity of the DMSO-treated group was set as 1. Error bars are ± SEM (n = 3). (*D*) Flow cytometry analysis of mitochondrial membrane potential effect of KA and apigenin evaluated by employing 5,5′,6,6′-Tetrachloro-1,1′,3,3′-tetraethyl-imidacarbocyanine iodide (JC-1). FL-1 channel, excitation wavelength 488 nm; emission wavelength 500 to 560 nm; FL-2 channel, excitation wavelength 488 nm, emission wavelength 550 to 600 nm. (*E*) MPO and GPX4 levels in control and treated groups that were examined by Western blots. (*F*) SH-SY5Y cells were preincubated with or without KA (500 μM, 12 h) and apigenin (20 μM, 12 h), and then images were taken by transmission electron microscopy. (Scale bar, 500 nm.) (*G*) Apigenin reduces the accumulation of lactate production caused by KA, as described in *SI Appendix*. The activity of lactate production of DMSO-treated cells was set as 1. Error bars are ± SEM (n = 5). (*H*) Apigenin reduces the increase in pyruvate kinase activity caused by KA as described in *SI Appendix*. The activity of pyruvate kinase of DMSO-treated cells was set as 1. Error bars are ± SEM (n = 5). Statistical analyses were performed with one-way ANOVA with multiple comparisons. $^{**}P < 0.01$, $^{***}P < 0.001$ vs. DMSO group.

brain. KA treatment induced an increase of oxidative stress in these cells, but we were delighted to observe that apigenin can effectively improve the antioxidative capability of these cells, including increasing levels of cellular GPX4, TrxR, and GSH; on the other hand, the expression of MPO and HClO can be suppressed (*SI Appendix*, Figs. S15–S17). Taken together, these results demonstrated that KA stimulation caused abnormal expression of MPO levels and resulted in a significant decrease of GPX4 expression, abnormal lipid peroxidation, and mitochondrial damage, eventually triggering ferroptotic cell death; fortunately, the screened apigenin by using HCP can relieve KA-induced ferroptosis and share neuroprotective functions in neural cells. Importantly, the enhanced antioxidant capabilities of these apigenin-activated neural cells and the dynamic changes of HClO fluxes during ferroptosis can be directly observed by this versatile HCP probe.

The BBB Permeability of HCP. Encouraged by the satisfactory performance of HCP in live-cell imaging, we attempted to investigate whether HCP can be used to monitor dynamic changes of endogenous HClO levels in epileptic brains of live animal models in vivo. An important prerequisite for brain imaging is that the probe should penetrate the BBB. Thus, the lipophilicity of HCP (log $P = 2.71$) was first tested, indicating that it might penetrate the BBB (54). To investigate and compare the actual BBB penetration of HCP with other representatively reported HClO probes (55, 56), we performed an in vitro parallel artificial membrane permeability assay of BBB (PAMPA-BBB) through the combined use of a microplate reader and HPLC. The results showed that the effective permeability of HCP ($P_e = 12.72$) was much higher than that of other HClO probes ($P_e < 8$) (*SI Appendix*, Fig. S18), suggesting a strong potential for BBB permeability of HCP. To further measure the content of the brain of HCP after i.v. injection with other HCP probes, we performed HPLC-MS/MS to determine the absolute permeability of HCP following the previously reported protocols (57). In vivo brain pharmacokinetic studies showed a good uptake of HCP by the brain (transport: 2.63% at 3 min), which is consistent with the in vitro PAMPA-BBB results. Moreover, we compared the relative penetrability ratios of other HClO probes (Gal-NAP, C7, R6G) to HCP after i.v. injection in mouse brains, which further confirmed the better BBB permeability of HCP than other probes (*SI Appendix*, Fig. S19).

In Vivo Imaging of HClO Fluxes in Brains of Epileptic Mice. To determine the potential of HCP for in vivo imaging of endogenous HClO fluxes under KA-induced neuronal stress rather than neuronal death (*SI Appendix*, Figs. S20 and S21), an epilepsy model of mice was established by i.p. injection of a low dose of KA (6 mg/kg) into wild-type (WT) mice, which is widely employed to study epileptic seizures (58). Apigenin (60 mg/kg) was injected in the early-prevention and late-treatment stages of epilepsy mice, respectively (Fig. 6*A*). Since trotting and searching are behaviors in which nearly all mice have the daily experience, we tested their ability to adapt to a new environment by performing an open-field test. To this end, we placed mice in a chamber and observed the effects of KA and apigenin on the locomotor activity of mice. As shown in Fig. 6*B*, the results encouraged our speculation; KA-treatment mice showed significantly reduced velocity into the total area and central regions and also apparently reduced the number of entries to the central area and the residence time in the central area. The less exploration behavior and more emotional stress showed the specific behavioral characteristics of epileptic mice. Strikingly, the prophylactic and therapeutic effects of apigenin are evident, which significantly improve KA-induced epileptic symptoms. After i.v. injection of HCP (0.5 mg/kg), in vivo imaging showed that the fluorescence intensity of the epilepsy group in the brain regions was significantly higher than that in WT healthy mice at different times (5, 15, 30, 45, and 60 min), clearly demonstrating HCP can effectively cross the BBB and track the up-regulation of HClO in the brain. Particularly, pre/posttreatment with apigenin, the mouse brains showed reduced fluorescence signals compared to those treated with KA alone (Fig. 6*C* and *SI Appendix*, Fig. S22). These results confirm that apigenin can effectively control the KA-induced overexpression of HClO in the epileptic brains, which are consistent with the behavioral results of pharmacological mouse models. Moreover, these in vivo imaging observations were also validated by the ex vivo fluorescence imaging of the brains from these mice (Fig. 6*D* and *SI Appendix*, Fig. S23). Furthermore, these observations were confirmed by in vivo and ex vivo fluorescent imaging with other reported HClO probes (*SI Appendix*, Fig. S24). Despite their weaker BBB permeability, the observed results were also consistent with the in vitro cellular staining results, strongly suggesting that the observed fluorescence intensity enhancement is indeed caused by the increased HClO fluxes in the epileptic brain. In addition, we managed to directly measure the endogenous HClO concentration in brain tissues using HCP. The prespiked HClO was used as the internal standard in the prepared fresh brain tissue homogenates. The spiked samples were incubated with HCP briefly for 30 s and then measured (*SI Appendix*, Fig. S25). The average HClO concentrations in the fresh brain tissue homogenates from WT and KA-induced epileptic mice have been determined to be 0.007 $\mu mol \cdot g^{-1}$ and 0.045 $\mu mol \cdot g^{-1}$ protein, respectively, in agreement with the estimate based on the previously reported endogenous H_2O_2 concentration and conversion rates of H_2O_2 to HClO in neurons (59, 60).

Imaging Brain Tissue Slices with Two-Photon Excitation. The measurement of the two-photon absorption cross-section (δ_2) showed a significant enhancement of the maximum action δ_2 values of HCP after reaction with HClO at 800 nm (*SI Appendix*, Fig. S2). This finding suggested that HCP was suitable for two-photon imaging, which is valuable for measuring thick brain tissue slices. Thus, fluorescence images of the brain slices were observed under two-photon excitation at 800 nm (*SI Appendix*, Fig. S26). Bright green fluorescence signals were clearly visualized with high signal to noise (S/N) ratios in epileptic mice down to 150 μm in-depth, confirming the great potential of HCP in deep-tissue two-photon brain imaging owing to its marked two-photon properties and brain tissue permeability. Importantly, after 60 min i.v. injection of HCP, a higher level of the aggregated HClO was observed in the Z-stack images of brain slices from the epileptic brains (Fig. 6 *E* and *F* and *SI Appendix*, Fig. S27); while treatment by apigenin can control the abnormal accumulation of chlorination stress. Taken together, these in vivo and ex vivo studies confirmed that HCP imaging provides a promising approach for in vivo brain monitoring of dynamic changes of endogenous HClO in live epileptic animals, which can provide insights into changes of chlorinated stress during treatment with antioxidant drugs. Moreover, apigenin may serve as a potential neuroprotective agent in the treatment of neurodegenerative diseases.

Neuroprotection of Apigenin by Regulation of KA-Induced Ferroptosis. Given that SIRT1, an NAD+-dependent deacetylase, plays a vital role in protecting neurons in various models of neurodegenerative disease (61), we thus asked whether MPO-generated HClO might have some association with SIRT1. To this end, we investigated the expression of these proteins in different treated mouse brains, by performing immunofluorescence studies on the largest surface of the hippocampus (Fig. 7 *A* and *B*). The Z-stack images of brain slices from mice stimulated by KA showed strong MPO fluorescence signals and relatively much weaker SIRT1 immunofluorescence, thereby leading to the up-regulation of Ac-p53 levels. Consistent with the pharmacological models of KA-induced

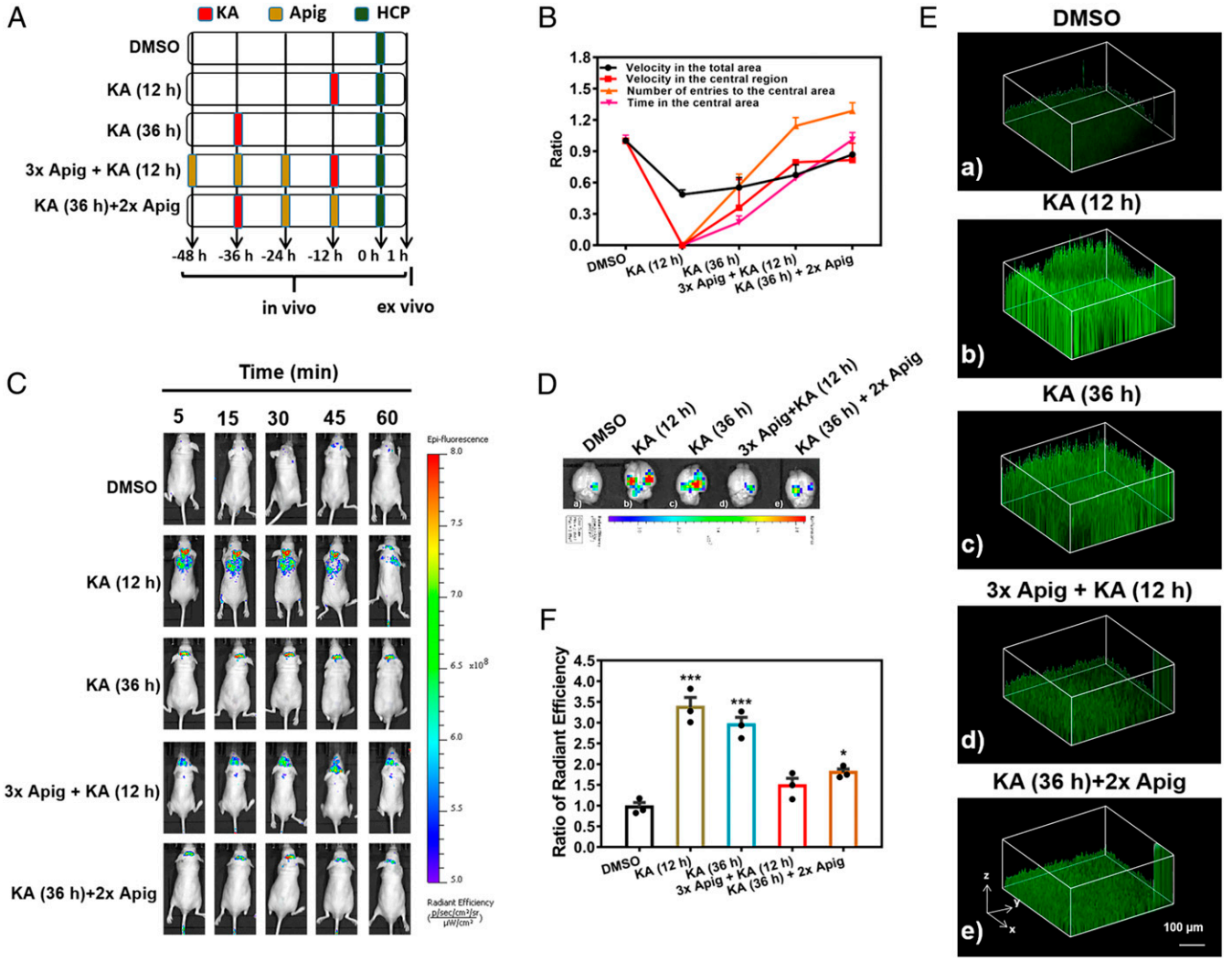

Fig. 6. In vivo and ex vivo fluorescence imaging with HCP. (*A*) The flowchart of mice treated with KA (6 mg/kg), apigenin (60 mg/kg), and HCP (10 μM). (*B*) Comparisons of the behavior of mice in each group via the open-field test. The velocity in the total area and central region, the number of entries to the central area, and time in the central area of DMSO-treated mice were set as 1. Error bars are ± SD ($n = 3$). (*C*) Fluorescence images of five groups of mice at 5, 15, 30, 45, and 60 min after i.v. injection with HCP, indicating that HCP was able to cross the BBB and image in live brains. Note that fluorescence signals in KA-induced epileptic brains were significantly higher than those in the control group, and treatment with apigenin could help to relieve the overexpressed HClO. (*D*) Ex vivo fluorescence images of relative ClO^- levels in mouse brains after 60 min postinjection of HCP using the IVIS Spectrum imaging system. (*E*) The two-photon fluorescence images of two-and-a-half-dimensional (2.5D) volume-rendered and different depths of maximum hippocampal surface in brain tissues from *D*. Green, HCP channel. Fluorescence excitation filter MP (multiple-photon) 800 nm, emission window 450 to 600 nm. (Scale bar, 100 μm.) (*F*) The relative ratio of fluorescence intensity of the brain sections shown in *E* was quantified by Image J. The fluorescence intensity of DMSO-treated mouse brain sections was set as 1. Statistical analyses were performed with one-way ANOVA with multiple comparisons; $*P < 0.05$, $***P < 0.001$ vs. DMSO-treated group. Error bars are ± SEM ($n = 3$).

epilepsy, we observed severe neural cell death, including disordered arrangement and loss of neural cells in all of the hippocampal subregions (*SI Appendix*, Fig. S28). On the contrary, the fluorescence of brain slices from the apigenin-treated mice exhibited a relatively weaker MPO but stronger SIRT1 immunofluorescence, indicating the down-regulation of MPO levels and a striking increase of SIRTI expression in the apigenin-treated groups. Importantly, we found that apigenin administration can efficiently protect the neural cells in the whole hippocampal regions, in agreement with the above observations of the decreased HClO generation. These findings suggested that the decreased activity of SIRT1 is accompanied by an excess of MPO expression, which is promoting the overgeneration of HClO and the accumulation of chlorinated stress. Strikingly, SIRT1 can be activated upon blocking of MPO and scavenging of the overexpression HClO by apigenin administration. The level of Ac-p53 inside the brains treated with apigenin was down-regulated, suggesting that the p53-mediated ferroptosis pathway might be blocked (62). Consistent with these correlations, we observed the obvious up-regulation of GPX4 in the apigenin-treated groups, suggesting the important roles of apigenin in the inhibition of ferroptosis of neural cells (Fig. 7*B*). Additionally, tissue proteins from the hippocampal areas and around cortical areas of the mouse brains were extracted for Western blotting analyses. The results further confirmed the up-regulated SIRT1 and GPX4 expression in apigenin-administration groups, which was accompanied by the dynamically decreased expression of MPO and increased expression of TrxR and GSH (Fig. 7*C* and *SI Appendix*, Figs. S29 and S30). To examine changes in the protein structure of SIRT1 under chlorinated stress, proteomics analyses were finally performed to identify the chlorinated reaction of SIRT1 after treatment with HClO or $MPO/H_2O_2/Cl^-$. Interestingly, Matrix-Assisted Laser Desorption Ionization-Time of Flight Mass Spectrometer (MALDI-TOF MS) analysis revealed that six tyrosine residues

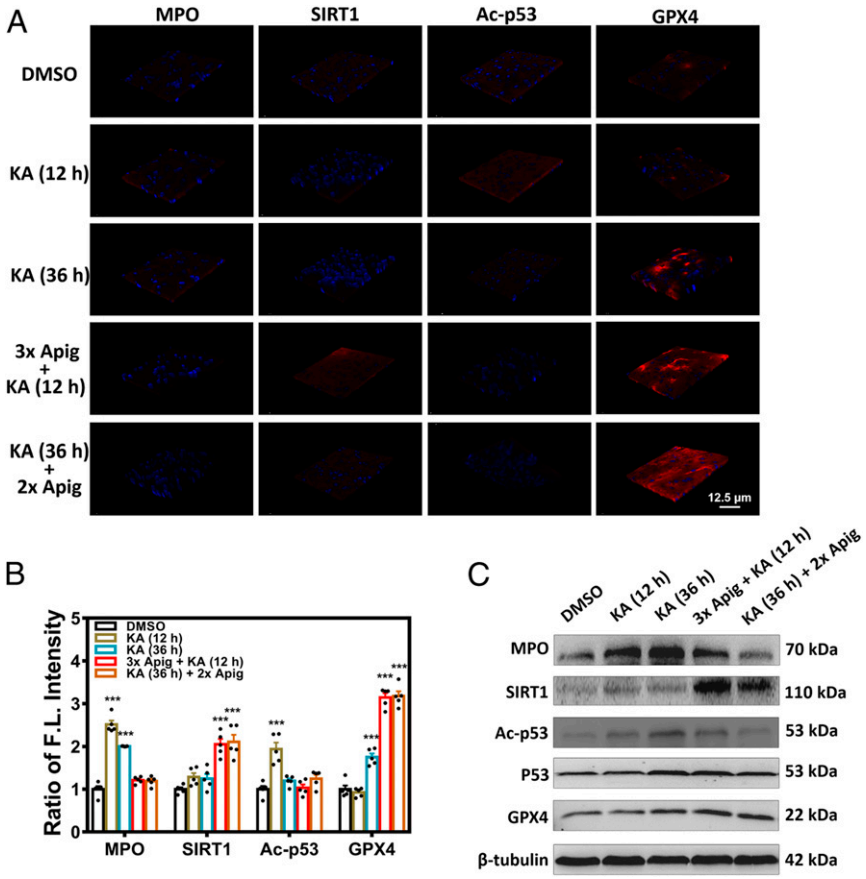

Fig. 7. (*A*) Immunofluorescence staining of MPO, SIRT1, Ac-p53, and GPX-4 on frozen sections of paired normal and treated mice from Fig. 6*D*. Blue, DAPI; red, Alexa Fluor 594-conjugated AffiniPure goat anti-rabbit/mouse IgG (H+L). (Scale bar, 12.5 μm.) (*B*) The relative ratio of immunofluorescence intensity shown in *A* was quantified by Image J. The expression of MPO, SIRT1, Ac-p53, and GPX4 of DMSO-treated mice quantified by immunofluorescence intensity was set as 1, respectively. Statistical analyses were performed with one-way ANOVA with multiple comparisons, $***P < 0.001$ vs. DMSO-treated group. Error bars are ± SEM ($n = 3$). (*C*) MPO, SIRT1, Ac-p53, p53, and GPX4 expressed levels of tissues in the hippocampal area of the mice were examined by Western blots.

(Tyr) in the total of eight Tyr sites of SIRT1 could be covalently modified by chlorination reaction, suggesting a redox-sensitive SIRT1 under chlorinated stress (*SI Appendix*, Fig. S31). These results provided evidence that an excess of exogenous HClO or MPO-generated endogenous HClO can lead to chlorinated damage to the structure of SIRT1, thus decreasing enzymatic activities and leading to protein degradation and further causing epileptic behaviors (63). Taken together, all these findings demonstrated that the KA stress induced up-regulation of MPO, accompanied by the reduced activities of SIRT1 and GPX4, while apigenin may serve as an efficient activator for SIRT1 and GPX4. Further, an MPO/SIRT1/p53 pathway might be a possible pathway for promoting neural cell death by ferroptosis during the pathogenesis of epilepsy.

Conclusions

Endogenous HClO generation by MPO plays a critical role in regulating cellular redox states and is widely implicated in neurodegenerative disorders. Therefore, a better understanding of its regulation in live brains is critical. By focusing on the MPO-mediated chlorinated stress in epileptic seizures, we describe a two-photon fluorescent probe for real-time tracking of endogenous HClO in live cells and in vivo, especially in live brains. This probe exhibited efficient BBB penetrability, high photostability, and excellent temporal and spatial resolution. This study enables the sensitive detection and imaging of HClO generation by MPO in live brains without interference from other biological species. Importantly, the dynamic changes of endogenous HClO fluxes in brains were directly monitored during the therapeutic process of KA-induced epileptic mice in vivo and ex vivo, suggesting a positive correlation between the MPO-mediated chlorinated stress and severe neuronal damage and epileptogenesis. Furthermore, by combining with high-content analysis, a simple high-throughput screening approach for antiepileptic agents was easily constructed, and apigenin was screened and confirmed as an efficient lead compound for epilepsy prevention and treatment. Further, we discovered that SIRT1 inactivation by MPO-generated HClO might be a possible pathological mechanism for epileptogenesis; while apigenin can relieve the MPO-mediated oxidative stress for inhibition of ferroptosis, thereby promoting the antiepileptic functions. This work not only provides a robust fluorescent tool for understanding the pathological mechanism of MPO-generated HClO fluxes associated with neurodegenerative disease, but also illustrates a versatile strategy for accelerating the discovery of small molecular agents for antiepileptic prevention and treatments.

Materials and Methods

Materials, methods, and chemical synthesis are described in *SI Appendix*. All mice were purchased from the Model Animal Research Centre of Nanjing University. All mice were maintained under specific pathogen-free conditions and used following the experimental animal guidelines set by the Institute of Animal Care and Use Committee. All animal experiments were approved by the Institutional Animal Care and Use Committee at Nanjing Normal University. Further details are provided in *SI Appendix*, which also includes detailed methods for all associated protocols, cell fluorescence imaging, and animal experiments. All data used in this study are publicly available in *SI Appendix*.

ACKNOWLEDGMENTS. This work is financially supported by the National Natural Science Foundation of China (21778033, 81803349), the program of Jiangsu Specially-Appointed Professor for Y. Qian, and the Open Project of State Key Laboratory of Pharmaceutical Biotechnology (KF-GN-202002). Gratitude is expressed to Prof. Pedro Brugarolas and Prof. Fei Sun for helpful reading and comments.

1. K. Pravalika *et al*., Myeloperoxidase and neurological disorder: A crosstalk. *ACS Chem. Neurosci.* **9**, 421–430 (2018).
2. J. Marcinkiewicz *et al*., Antimicrobial and cytotoxic activity of hypochlorous acid: Interactions with taurine and nitrite. *Inflamm. Res.* **49**, 280–289 (2000).
3. F. C. Fang, Antimicrobial reactive oxygen and nitrogen species: Concepts and controversies. *Nat. Rev. Microbiol.* **2**, 820–832 (2004).
4. V. E. Kagan *et al*., Carbon nanotubes degraded by neutrophil myeloperoxidase induce less pulmonary inflammation. *Nat. Nanotechnol.* **5**, 354–359 (2010).
5. J. Everse, P. W. Coates, Role of peroxidases in Parkinson disease: A hypothesis. *Free Radic. Biol. Med.* **38**, 1296–1310 (2005).
6. I. Tasset *et al*., NGF and nitrosative stress in patients with Huntington's disease. *J. Neurol. Sci.* **315**, 133–136 (2012).
7. N. Stefanova, B. Georgievska, H. Eriksson, W. Poewe, G. K. Wenning, Myeloperoxidase inhibition ameliorates multiple system atrophy-like degeneration in a transgenic mouse model. *Neurotox. Res.* **21**, 393–404 (2012).
8. D. K. Choi *et al*., Ablation of the inflammatory enzyme myeloperoxidase mitigates features of Parkinson's disease in mice. *J. Neurosci.* **25**, 6594–6600 (2005).
9. R. Forghani *et al*., Myeloperoxidase propagates damage and is a potential therapeutic target for subacute stroke. *J. Cereb. Blood Flow Metab.* **35**, 485–493 (2015).
10. Y. Zhang *et al*., Myeloperoxidase nuclear imaging for epileptogenesis. *Radiology* **278**, 822–830 (2016).
11. C. G. Bien *et al*., Pathogenesis, diagnosis and treatment of Rasmussen encephalitis: A European consensus statement. *Brain* **128**, 454–471 (2005).
12. H. Li, X. Li, W. Shi, Y. Xu, H. Ma, Rationally designed fluorescence· OH probe with high sensitivity and selectivity for monitoring the generation of· OH in iron autoxidation without addition of H_2O_2. *Angew. Chem. Int. Ed. Engl.* **57**, 12830–12834 (2018).
13. A. T. Wrobel, T. C. Johnstone, A. Deliz Liang, S. J. Lippard, P. Rivera-Fuentes, A fast and selective near-infrared fluorescent sensor for multicolor imaging of biological nitroxyl (HNO). *J. Am. Chem. Soc.* **136**, 4697–4705 (2014).
14. R. Zhang *et al*., Real-time discrimination and versatile profiling of spontaneous reactive oxygen species in living organisms with a single fluorescent probe. *J. Am. Chem. Soc.* **138**, 3769–3778 (2016).
15. C. Yik-Sham Chung, G. A. Timblin, K. Saijo, C. J. Chang, Versatile histochemical approach to detection of hydrogen peroxide in cells and tissues based on puromycin staining. *J. Am. Chem. Soc.* **140**, 6109–6121 (2018).
16. T. I. Kim, B. Hwang, B. Lee, J. Bae, Y. Kim, Selective monitoring and imaging of eosinophil peroxidase activity with a J-aggregating probe. *J. Am. Chem. Soc.* **140**, 11771–11776 (2018).
17. X. Li *et al*., Visualizing peroxynitrite fluxes in endothelial cells reveals the dynamic progression of brain vascular injury. *J. Am. Chem. Soc.* **137**, 12296–12303 (2015).
18. X. Wang *et al*., Illuminating the function of the hydroxyl radical in the brains of mice with depression phenotypes by two-photon fluorescence imaging. *Angew. Chem. Int. Ed. Engl.* **58**, 4674–4678 (2019).
19. Y. Qian, M. Schürmann, P. Janning, C. Hedberg, H. Waldmann, Activity-based proteome profiling probes based on Woodward's Reagent K with distinct target selectivity. *Angew. Chem. Int. Ed. Engl.* **55**, 7766–7771 (2016).
20. Z. Li, Y. Xu, H. Zhu, Y. Qian, Imaging of formaldehyde in plants with a ratiometric fluorescent probe. *Chem. Sci. (Camb.)* **8**, 5616–5621 (2017).
21. S. Kenmoku, Y. Urano, H. Kojima, T. Nagano, Development of a highly specific rhodamine-based fluorescence probe for hypochlorous acid and its application to real-time imaging of phagocytosis. *J. Am. Chem. Soc.* **129**, 7313–7318 (2007).
22. Q. A. Best, N. Sattenapally, D. J. Dyer, C. N. Scott, M. E. McCarroll, pH-dependent Si-fluorescein hypochlorous acid fluorescent probe: Spirocycle ring-opening and excess hypochlorous acid-induced chlorination. *J. Am. Chem. Soc.* **135**, 13365–13370 (2013).
23. H. Zhu, J. Fan, J. Wang, H. Mu, X. Peng, An "enhanced PET"-based fluorescent probe with ultrasensitivity for imaging basal and elesclomol-induced HClO in cancer cells. *J. Am. Chem. Soc.* **136**, 12820–12823 (2014).
24. M. Sun *et al*., Oxidative cleavage-based near-infrared fluorescent probe for hypochlorous acid detection and myeloperoxidase activity evaluation. *Anal. Chem.* **86**, 671–677 (2014).
25. L. Zhou *et al*., Molecular engineering of a TBET-based two-photon fluorescent probe for ratiometric imaging of living cells and tissues. *J. Am. Chem. Soc.* **136**, 9838–9841 (2014).
26. H. M. Kim, B. R. Cho, Small-molecule two-photon probes for bioimaging applications. *Chem. Rev.* **115**, 5014–5055 (2015).
27. M. Cui *et al*., Smart near-infrared fluorescence probes with donor-acceptor structure for in vivo detection of β-amyloid deposits. *J. Am. Chem. Soc.* **136**, 3388–3394 (2014).
28. D. Kim *et al*., Two-photon absorbing dyes with minimal autofluorescence in tissue imaging: Application to in vivo imaging of amyloid-β plaques with a negligible background signal. *J. Am. Chem. Soc.* **137**, 6781–6789 (2015).
29. S. W. Wang, F. Hu, Y. T. Pan, L. G. Ng, B. Liu, Bright AIEgen-protein hybrid nanocomposite for deep and high-resolution in vivo two-photon brain imaging. *Adv. Funct. Mater.* **29**, 1902717 (2019).
30. Z. Mao *et al*., Design of a ratiometric two-photon probe for imaging of hypochlorous acid (HClO) in wounded tissues. *Chem. Sci.* **9**, 6035–6040 (2018).
31. B. Zhu *et al*., Highly specific and ultrasensitive two-photon fluorescence imaging of native HOCl in lysosomes and tissues based on thiocarbamate derivatives. *Anal. Chem.* **88**, 12532–12538 (2016).
32. J. J. Hu *et al*., HKOCl-3: A fluorescent hypochlorous acid probe for live-cell and *in vivo* imaging and quantitative application in flow cytometry and a 96-well microplate assay. *Chem. Sci.* **7**, 2094–2099 (2016).
33. P. Wei *et al*., Deformylation reaction-based probe for *in vivo* imaging of HOCl. *Chem. Sci.* **9**, 495–501 (2017).
34. Q. Xu *et al*., Development of imidazoline-2-thiones based two-photon fluorescence probes for imaging hypochlorite generation in a co-culture system. *Angew. Chem. Int. Ed. Engl.* **54**, 4890–4894 (2015).
35. L. Yuan *et al*., Development of targetable two-photon fluorescent probes to image hypochlorous acid in mitochondria and lysosome in live cell and inflamed mouse model. *J. Am. Chem. Soc.* **137**, 5930–5938 (2015).
36. Q. Xu *et al*., A selective imidazoline-2-thione-bearing two-photon fluorescent probe for hypochlorous acid in mitochondria. *Anal. Chem.* **88**, 6615–6620 (2016).
37. Y. W. Jun *et al*., A two-photon fluorescent probe for ratiometric imaging of endogenous hypochlorous acid in live cells and tissues. *Chem. Commun. (Camb.)* **53**, 10800–10803 (2017).
38. X. Zhang *et al*., Design and synthesis of curcumin analogues for in vivo fluorescence imaging and inhibiting copper-induced cross-linking of amyloid beta species in Alzheimer's disease. *J. Am. Chem. Soc.* **135**, 16397–16409 (2013).
39. J. Chan, S. C. Dodani, C. J. Chang, Reaction-based small-molecule fluorescent probes for chemoselective bioimaging. *Nat. Chem.* **4**, 973–984 (2012).
40. E. A. Lemke, C. Schultz, Principles for designing fluorescent sensors and reporters. *Nat. Chem. Biol.* **7**, 480–483 (2011).
41. Q. Li *et al*., Solid-phase synthesis of styryl dyes and their application as amyloid sensors. *Angew. Chem. Int. Ed. Engl.* **43**, 6331–6335 (2004).
42. C. H. Kim *et al*., Nuclear receptor Nurr1 agonists enhance its dual functions and improve behavioral deficits in an animal model of Parkinson's disease. *Proc. Natl. Acad. Sci. U.S.A.* **112**, 8756–8761 (2015).
43. C. L. Fu, L. S. Hsu, Y. F. Liao, M. K. Hu, New hydroxyquinoline-based derivatives as potent modulators of amyloid-β aggregations. *Arch. Pharm. (Weinheim)* **349**, 327–341 (2016).
44. M. Chioua *et al*., Novel quinolylnitrones combining neuroprotective and antioxidant properties. *ACS Chem. Neurosci.* **10**, 2703–2706 (2019).
45. M. Chioua *et al*., New quinolylnitrones for stroke therapy: Antioxidant and neuroprotective (Z)- N- tert-Butyl-1-(2-chloro-6-methoxyquinolin-3-yl)methanimine oxide as a new lead-compound for ischemic stroke treatment. *J. Med. Chem.* **62**, 2184–2201 (2019).
46. C. G. Dai, J. L. Wang, Y. L. Fu, H. P. Zhou, Q. H. Song, Selective and real-time detection of nitric oxide by a two-photon fluorescent probe in live cells and tissue slices. *Anal. Chem.* **89**, 10511–10519 (2017).
47. H. Kobayashi, M. Ogawa, R. Alford, P. L. Choyke, Y. Urano, New strategies for fluorescent probe design in medical diagnostic imaging. *Chem. Rev.* **110**, 2620–2640 (2010).
48. A. N. Mayeno, A. J. Curran, R. L. Roberts, C. S. Foote, Eosinophils preferentially use bromide to generate halogenating agents. *J. Biol. Chem.* **264**, 5660–5668 (1989).
49. C. Manach, A. Scalbert, C. Morand, C. Rémésy, L. Jiménez, Polyphenols: Food sources and bioavailability. *Am. J. Clin. Nutr.* **79**, 727–747 (2004).
50. D. W. Choi, Glutamate neurotoxicity and diseases of the nervous system. *Neuron* **1**, 623–634 (1988).
51. M. Lévesque, M. Avoli, The kainic acid model of temporal lobe epilepsy. *Neurosci. Biobehav. Rev.* **37**, 2887–2899 (2013).
52. W. S. Yang *et al*., Peroxidation of polyunsaturated fatty acids by lipoxygenases drives ferroptosis. *Proc. Natl. Acad. Sci. U.S.A.* **113**, E4966–E4975 (2016).
53. W. S. Yang *et al*., Regulation of ferroptotic cancer cell death by GPX4. *Cell* **156**, 317–331 (2014).
54. H. Pajouhesh, G. R. Lenz, Medicinal chemical properties of successful central nervous system drugs. *NeuroRx* **2**, 541–553 (2005).
55. M. A. Choi *et al*., Design, synthesis and biological evaluation of a series of CNS penetrant HDAC inhibitors structurally derived from amyloid-β probes. *Sci. Rep.* **9**, 13187 (2019).
56. J. Yang *et al*., Oxalate-curcumin-based probe for micro- and macroimaging of reactive oxygen species in Alzheimer's disease. *Proc. Natl. Acad. Sci. U.S.A.* **114**, 12384–12389 (2017).
57. L. J. Zhu *et al*., CAPON-nNOS coupling can serve as a target for developing new anxiolytics. *Nat. Med.* **20**, 1050–1054 (2014).
58. J. A. Miller *et al*., Repeated exposure to low doses of kainic acid activates nuclear factor kappa B (NF-κB) prior to seizure in transgenic NF-κB/EGFP reporter mice. *Neurotoxicology* **44**, 39–47 (2014).
59. M. Spanos *et al*., Quantitation of hydrogen peroxide fluctuations and their modulation of dopamine dynamics in the rat dorsal striatum using fast-scan cyclic voltammetry. *ACS Chem. Neurosci.* **4**, 782–789 (2013).
60. T. M. Jeitner *et al*., Inflaming the diseased brain: A role for tainted melanins. *Biochim. Biophys. Acta* **1852**, 937–950 (2015).
61. F. Zhang *et al*., Protective effects and mechanisms of sirtuins in the nervous system. *Prog. Neurobiol.* **95**, 373–395 (2011).
62. S. J. Wang *et al*., Acetylation is crucial for p53-mediated ferroptosis and tumor suppression. *Cell Rep.* **17**, 366–373 (2016).
63. X. Wan, J. J. Wen, S. J. Koo, L. Y. Liang, N. J. Garg, SIRT1-PGC1α-NFκB pathway of oxidative and inflammatory stress during Trypanosoma cruzi infection: Benefits of SIRT1-targeted therapy in improving heart function in Chagas disease. *PLoS Pathog.* **12**, e1005954 (2016).